Angular dependence of light trapping in nanophotonic thin-film solar cells

Michael Smeets,[1,*] Vladimir Smirnov,[1] Karsten Bittkau,[1] Matthias Meier,[1] Reinhard Carius,[1] Uwe Rau[1] and Ulrich W. Paetzold[1,2]

[1]IEK5 – Photovoltaik, Forschungszentrum Juelich GmbH, D - 52425 Juelich, Germany
[2]IMEC v.z.w., Kapeldreef 75, 3001 Leuven, Belgium
**m.smeets@fz-juelich.de*

Abstract: The angular dependence of light-trapping in nanophotonic thin-film solar cells is inherent due to the wavelength-scale dimensions of the periodic nanopatterns. In this paper, we experimentally investigate the dependence of light coupling to waveguide modes for light trapping in a-Si:H solar cells deposited on nanopatterned back contacts. First, we accurately determine the spectral positions of individual waveguide modes in thin-film solar cells in external quantum efficiency and absorptance. Second, we demonstrate the strong angular dependence of this spectral position for our solar cells. Third, a moderate level of disorder is introduced to the initially periodic nanopattern of the back contacts. As a result, the angular dependence is reduced. Last, we experimentally compare this dependence on the angle of incidence for randomly textured, 2D periodically nanopatterned and 2D disordered back contacts in external quantum efficiency and short-circuit current density.

OCIS codes: (040.5350) Photovoltaic; (050.1950) Diffraction gratings; (050.6624) Subwavelength structures; (240.5440) Polarization-selective devices.

References

1. M. A. Green, *Solar cells—Operating Principles, Technology and System Applications* (Prentice-Hall, 1986).
2. J. Müller, B. Rech, J. Springer, and M. Vanecek, "TCO and light trapping in silicon thin film solar cells," Sol. Energy **77**(6), 917–930 (2004).
3. M. Kambe, A. Takahashi, N. Taneda, K. Masumo, T. Oyama, and K. Sato, "Fabrication of A-Si:H Solar cells on high haze SnO_2:F thin films," in 2008 33rd IEEE Photovoltaic Specialists Conference (IEEE, 2008), pp. 1–4.
4. C. Eisele, C. E. Nebel, and M. Stutzmann, "Periodic light coupler gratings in amorphous thin film solar cells," J. Appl. Phys. **89**(12), 7722 (2001).
5. V. E. Ferry, L. A. Sweatlock, D. Pacifici, and H. A. Atwater, "Plasmonic nanostructure design for efficient light coupling into solar cells," Nano Lett. **8**(12), 4391–4397 (2008).
6. R. Biswas, J. Bhattacharya, B. Lewis, N. Chakravarty, and V. Dalal, "Enhanced nanocrystalline silicon solar cell with a photonic crystal back-reflector," Sol. Energy Mater. Sol. Cells **94**(12), 2337–2342 (2010).
7. K. R. Catchpole and A. Polman, "Plasmonic solar cells," Opt. Express **16**(26), 21793–21800 (2008).
8. U. W. Paetzold, E. Moulin, D. Michaelis, W. Böttler, C. Wächter, V. Hagemann, M. Meier, R. Carius, and U. Rau, "Plasmonic reflection grating back contacts for microcrystalline silicon solar cells," Appl. Phys. Lett. **99**(18), 181105 (2011).
9. K. Söderström, F.-J. Haug, J. Escarré, O. Cubero, and C. Ballif, "Photocurrent increase in n-i-p thin film silicon solar cells by guided mode excitation via grating coupler," Appl. Phys. Lett. **96**(21), 213508 (2010).
10. V. E. Ferry, M. A. Verschuuren, H. B. T. Li, E. Verhagen, R. J. Walters, R. E. I. Schropp, H. A. Atwater, and A. Polman, "Light trapping in ultrathin plasmonic solar cells," Opt. Express **18**(S2), A237–A245 (2010).
11. R. Dewan and D. Knipp, "Light trapping in thin-film silicon solar cells with integrated diffraction grating," J. Appl. Phys. **106**(7), 074901 (2009).
12. C. Battaglia, C.-M. M. Hsu, K. Söderström, J. Escarré, F.-J. J. Haug, M. Charrière, M. Boccard, M. Despeisse, D. T. L. Alexander, M. Cantoni, Y. Cui, and C. Ballif, "Light trapping in solar cells: can periodic beat random?" ACS Nano **6**(3), 2790–2797 (2012).
13. P. Mialhe, S. Mouhamed, and A. Haydar, "The solar cell output power dependence on the angle of incident radiation," Renew. Energy **1**(3-4), 519–521 (1991).
14. A. Heinämäki and G. Guekos, "Solar cell short-circuit current dependence on the angle of the incident radiation," Solar Cells **20**(1), 65–73 (1987).

#240779 Received 12 May 2015; revised 19 Sep 2015; accepted 12 Oct 2015; published 23 Oct 2015

15. A. Parretta, A. Sarno, P. Tortora, H. Yakubu, P. Maddalena, J. Zhao, and A. Wang, "Angle-dependent reflectance measurements on photovoltaic materials and solar cells," Opt. Commun. **172**(1-6), 139–151 (1999).
16. I. Tobías, A. Luque, and A. Martí, "Light intensity enhancement by diffracting structures in solar cells," J. Appl. Phys. **104**(3), 034502 (2008).
17. Z. Yu, A. Raman, and S. Fan, "Fundamental limit of nanophotonic light trapping in solar cells," Proc. Natl. Acad. Sci. U.S.A. **107**(41), 17491–17496 (2010).
18. A. Naqavi, K. Söderström, F.-J. Haug, V. Paeder, T. Scharf, H. P. Herzig, and C. Ballif, "Understanding of photocurrent enhancement in real thin film solar cells: towards optimal one-dimensional gratings," Opt. Express **19**(1), 128–140 (2011).
19. A. Naqavi, F. J. Haug, K. Söderström, C. Battaglia, V. Paeder, T. Scharf, H. P. Herzig, and C. Ballif, "Angular behavior of the absorption limit in thin film silicon solar cells," Prog. Photovolt. Res. Appl. **1002**, 2371 (2013).
20. U. W. Paetzold, M. Smeets, M. Meier, K. Bittkau, T. Merdzhanova, V. Smirnov, D. Michaelis, C. Waechter, R. Carius, and U. Rau, "Disorder improves nanophotonic light trapping in thin-film solar cells," Appl. Phys. Lett. **104**(13), 131102 (2014).
21. M. Smeets, V. Smirnov, M. Meier, K. Bittkau, R. Carius, U. Rau, and U. W. Paetzold, "On the geometry of plasmonic reflection grating back contacts for light trapping in prototype amorphous silicon thin-film solar cells," J. Photonics Energy **5**(1), 057004 (2014).
22. F.-J. Haug, K. Söderström, A. Naqavi, and C. Ballif, "Resonances and absorption enhancement in thin film silicon solar cells with periodic interface texture," J. Appl. Phys. **109**(8), 084516 (2011).
23. K. R. Catchpole and A. Polman, "Design principles for particle plasmon enhanced solar cells," Appl. Phys. Lett. **93**(19), 191113 (2008).
24. U. W. Paetzold, E. Moulin, B. E. Pieters, R. Carius, and U. Rau, "Design of nanostructured plasmonic back contacts for thin-film silicon solar cells," Opt. Express **19**(6), A1219–A1230 (2011).
25. M. Meier, U. W. Paetzold, M. Prömpers, T. Merdzhanova, R. Carius, and A. Gordijn, "UV nanoimprint for the replication of etched ZnO:Al textures applied in thin-film silicon solar cells," Prog. Photovolt. Res. Appl. **22**(12), 1226–1236 (2013).
26. U. W. Paetzold, W. Zhang, M. Prömpers, J. Kirchhoff, T. Merdzhanova, S. Michard, R. Carius, A. Gordijn, and M. Meier, "Thin-film silicon solar cell development on imprint-textured glass substrates," Mater. Sci. Eng. B **178**(9), 617–622 (2013).
27. V. Smirnov, C. Das, T. Melle, A. Lambertz, M. Hülsbeck, R. Carius, and F. Finger, "Improved homogeneity of microcrystalline absorber layer in thin-film silicon tandem solar cells," Mater. Sci. Eng. B **159–160**, 44–47 (2009).
28. S. Faÿ, J. Steinhauser, N. Oliveira, E. Vallat-Sauvain, and C. Ballif, "Opto-electronic properties of rough LP-CVD ZnO:B for use as TCO in thin-film silicon solar cells," Thin Solid Films **515**(24), 8558–8561 (2007).
29. K. Bittkau, W. Böttler, M. Ermes, V. Smirnov, and F. Finger, "Light scattering at textured back contacts for n-i-p thin-film silicon solar cells," J. Appl. Phys. **111**(8), 083101 (2012).

1. Introduction

Optically thin absorber layers for photovoltaic devices require efficient light trapping, in order to maintain high power conversion efficiencies. Commercial light-trapping concepts are based on scattering light at random textures at the front contacts and the back contacts of solar cells [1–3]. In recent years, a large number of nanophotonic light-trapping concepts have been proposed and implemented [4–9]. These nanophotonic concepts make use of light coupling to leaky waveguide modes located in the region of intermediate absorption of the absorber material of the solar cells. Such nanophotonic prototype solar cells focused on in our study apply nanopatterned back contacts. In previous studies, it was found that solar cells applying optimized nanophotonic nanopatterns reach similar or even superior power conversion efficiencies compared to solar cells with conventional random textures [6,10–12]. So far, these experimental studies have mostly been restricted to an evaluation of light trapping for light impinging at normal incidence. However, the general dependence of light trapping on the angle of incidence is well known for various concepts [13–16]. The apparent consequences could be limitations of the outdoor applicability of nanophotonic light-trapping concepts due to the angular dependence [13]. In particular, for periodic nanopatterns the impact of the angle of incidence for light trapping is expected to be relevant, since the applied nanopatterns are diffractive elements in the dimension of the optical wavelengths, which are responsible for the wavevector transfer. Up to date, the theory was analyzed in some investigations [5,17–19] and also excellent experimental realizations, concerning the angular dependence of nanophotonic light trapping were published [4,9,10]. Namely, the results of Söderström et al. support the fact that light trapping with 1-D periodically textured substrates

#240779 Received 12 May 2015; revised 19 Sep 2015; accepted 12 Oct 2015; published 23 Oct 2015

is mainly driven by scattering and diffraction of light larger than the angle of total internal reflection. Therefore, they resolve waveguide modes by coupling polarized light to the waveguide modes and compare the results to dispersion plots. The results of Ferry et al. go into the same direction, but they apply a 2-D periodic grating to couple the light to waveguide modes. They dispense with polarized measurements and compare the resonances they observe with simulations. In contrast to their results, we will focus on the impact of the angular and polarization dependence on resonance shift and thereby the short-circuit current densities. Based on these we introduce Gaussian disorder in our device and characterize how Gaussian disorder affects the angular and polarization dependences. This provides a much deeper insight in the role of waveguide modes for light trapping in solar cells as well as the impact of disorder on the light coupling to these waveguide modes.

The prototype devices focused on during our study are amorphous silicon thin-film solar cells deposited on 2D periodically nanopatterned back contacts. We apply amorphous silicon as an absorber material as the light trapping concepts and fabrication processes of the nanopatterned interfaces are supposed to be well applicable to other photovoltaic thin-film technologies like CIGS or organic photovoltaics.

Figure 1(a) shows a cross-section of a representative solar cell. Such solar cells have been described in the literature [10,20,21]. Details on the applied layer stack are provided in section 2. The light-trapping concept of these nanophotonic solar cells can be described as follows: Light passing the front contact of the solar cell or impinging the Ag back contact is diffracted at the periodic nanopatterns to defined angles. Multiple diffraction and reflection at both contacts result in guiding incident light, as an electromagnetic wave, inside the solar cell. This characteristic of nanophotonic light trapping with periodic nanopatterns postulates two requirements: (i) the light is diffracted to angles larger than the angle of total internal reflection at the front interface and (ii) after each reflection at the back contact the electromagnetic waves must share the same phase with the original electromagnetic wave diffracted at the back contact [22]. Nevertheless, considering the reciprocity of all light paths, light coupled to the waveguide mode can couple out to the ambient, as well. Thus, guiding light inside the nanophotonic solar cell is often described as coupling light to leaky waveguide modes of the absorber layer.

Since we apply Ag back contacts in the prototype solar cells, an Ag nanopattern in the dimension of the optical wavelengths is formed at the rear side. At such Ag nanopatterns, localized surface plasmon polaritons (*LSPP*), which represent resonances of collective charge carrier oscillations are excited at the nanostructures by the oscillating electromagnetic field of the incident light [23,24]. The radiative decay of the *LSPP*s results in efficient scattering of incident light [24]. Thus, the *LSPP* enhance the light-diffraction effect of the Ag nanopatterns. We call the *LSPP* supported Ag nanopattern: plasmonic reflection grating back contact (*PRGBC*).

In order to study the angular dependence of nanophotonic light trapping, we monitor the coupling to individual leaky waveguide modes dependent on the angle of incidence for different wavelengths and polarizations. Different polarizations are necessary as this allows for the separation of transversal electric and transversal magnetic waveguide modes. This leads to much better pronounced resonances in the EQE measurements. In addition, we introduce disorder to the periodic arrangement which broaden the wavevector transfer. As a result, introducing disorder improves the overall light trapping by reducing the spectral selectivity of light coupling to individual waveguide modes [10,12,20]. Due to this reduced spectral selectivity we observe smaller shifts of the coupling wavelengths. In a last step, we quantify the impact of the angular dependence on the optical and electrical performance of thin-film solar cells with (i) conventionally randomly, (ii) periodically and (iii) disordered back contacts. Therefore, the J_{SC} and EQE of solar cells with these three kinds of back contacts are taken as the figures of merit.

#240779 Received 12 May 2015; revised 19 Sep 2015; accepted 12 Oct 2015; published 23 Oct 2015

2. Experimental

Single junction a-Si:H thin-film solar cells with textured back contacts in substrate configuration are the central test-devices of this study and differently structured back contacts are compared. The conventionally randomly textured back contacts are processed on glass substrates covered with an, as-grown textured, SnO_2:F layer, provided by the Asahi Glass Company. The nanopatterned back contacts are processed on a glass substrate via ultra-violet nanoimprint lithography.

2.1 Ultra-violet nanoimprint lithography

In order to process the nanopatterned back contacts, ultra-violet nanoimprint lithography (UV-NIL) is applied. In this contribution, first, a glass-like resist ("Ormocomp" provided by "micro resist technology") is spin coated on a Corning glass substrate. Subsequently, a nanostructured soft mold with nanopatterned areas of a size of 6 mm x 6 mm, is pressed into the resist. These nanopatterned areas will define the solar cell area. The surface texture consists of nanopillars with a width around 150 nm, a height around 150 nm and a period of 500 nm. After hardening the imprint resist by illumination with ultra-violet light, the mold is removed and the inverse textures of the nanostructured mold is transferred into the imprint resist. Detailed information on this process are given elsewhere [25,26]. Same as for the randomly textured back contacts, an Ag layer with a thickness of 250 nm and a ZnO:Al layer with a thickness of 80 nm is deposited on the imprinted nanostructures, in order to form the *PRGBC*s.

2.2 Thin-film solar cell deposition sequence

In Fig. 1(a) a scanning electron microscopy (*SEM*) image of a representative solar cell with *PRGBC* is shown. The imprinted substrate, the Ag layer and ZnO:Al layer are shown. The corresponding layer thicknesses are 250 nm and 80 nm, respectively. Subsequently to the back contact, thin-film solar cells made of hydrogenated amorphous silicon (*a*-Si:H) are deposited as follows: First, a layer stack consisting of n-doped, intrinsic and p-doped *a*-Si:H is deposited by plasma enhanced chemical vapor deposition (*PECVD*). The thickness of the intrinsic layer is around 280 nm. Details concerning this process can be found elsewhere [27]. In a second step, ITO with a thickness of around 80 nm is sputtered as a front contact of the thin-film solar cell. Lastly, an Ag grid with finger width around 100 µm, periods in the mm-range and a finger thickness of 700 nm is evaporated. The Ag grid is not shown in Fig. 1(a). In order to complete the process, the thin-film solar cells are heated for 30 minutes at 160 °C. The same deposition routine is used for the randomly textured substrates.

2.3 Thin-film solar cell characterization

For the optical characterization, a LAMBDA950 spectrophotometer (Perkin Elmer) with integrating sphere was used. The main task is measuring the absorptance of the devices under an angle of eight degrees, calculated by $A = 1\text{-}R$, where A is the absorptance and R is the reflectance. The determination of the electrical properties, in particular fill factor (*FF*), open-circuit voltage (V_{OC}), short-circuit current density (J_{SC}) and power conversion efficiency (η) is realized by a WACOM-WXS-140s-super (Class A) AM 1.5 sun simulator and differential spectral response setup based on a grating monochromator. *FF* and V_{OC} are taken from sun simulator measurements, while the J_{SC} is calculated based on external quantum efficiency (*EQE*) measurements performed with a lens, in order to display the exit slit of the monochromator again with its smaller size. We use the J_{EQE} in order to guarantee highest accuracy during the determination of the current density. In the following, we will name the calculated current density: J_{SC}. It should be mentioned, that effects shown in the next sections were reproduced several times.

#240779 Received 12 May 2015; revised 19 Sep 2015; accepted 12 Oct 2015; published 23 Oct 2015

3. Results and discussion

In this chapter, we analyze the angular dependence of light coupling to leaky waveguide modes in hydrogenated amorphous silicon (a-Si:H) thin-film solar cells with *PRGBC*s. Coupling light to leaky waveguide modes results in spectrally sharp resonances in the absorptance (*A*). First, we resolve these resonances in the *A* and the *EQE*. Second, the spectral position of these resonances is determined, while varying the angle of incidence. Third, the angular dependence of light trapping for solar cells with periodically nanopatterned back contacts is compared to (i) conventionally randomly textured back contacts and (ii) nanopatterned back contacts, with intentionally introduced disorder to the *PRGBC*.

3.1. Coupling light to leaky waveguide modes in periodically nanopatterned solar cells

The concept of light trapping with *PRGBC*s significantly differs from conventionally applied light trapping with random textures. In the following, *EQE* and *A* of both concepts are compared. Therefore, Fig. 1(b) shows the *EQE* and *A* of a-Si:H thin-film solar cells with three types of back contacts, namely (i) flat, (ii) randomly textured and (iii) periodically nanopatterned back contacts, as a function of the wavelength between 300 nm and 800 nm. The period of the periodically nanopatterned back contact is 500 nm. Former studies [21] showed that applying this period allows for exciting a high number of waveguide modes, resulting in effective light trapping. We label the corresponding measurement curves by *SEM* images of the topography of the back contacts. In the wavelength range between 300 nm and 550 nm, light is mostly absorbed in a 280 nm thick a-Si:H layer during a single path. Thus, the optical response of the solar cell in this wavelength range solely depends on the light incoupling at the front interface. In Fig. 1(a) it can be seen that there is still a front contact structure left, after the deposition of the absorber layer. Nevertheless, the incoupling of light of short wavelengths is similar for the different patterned solar cells as well as the flat, as can be seen in Fig. 1(b) due to very similar EQEs. Our explanation for the similar behavior in incoupling is that the front contact structure is mainly dominated by the growth of the amorphous silicon and not by the substrates. The *EQE* increases from 12% around 300 nm to 85% around 550 nm. Same trend were reproduced by the absorptance measurements of the solar cells. Therefore, we assume that the front contact texture is mainly given by the growth of a-Si:H rather than the back

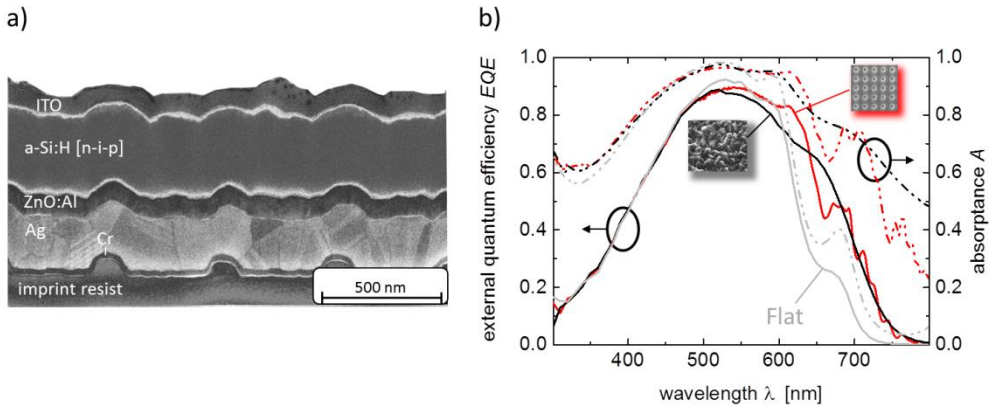

Fig. 1. a) Scanning electron microscopy (*SEM*) image of the cross-section of a hydrogenated amorphous silicon thin-film solar cell in substrate configuration with a plasmonic reflection grating back contact (*PRGBC*). b) External quantum efficiency (*EQE*)(full lines) and absorptance (*A*)(dotted lines) of thin-film solar cells with the layer stack shown in a). The back contact is either periodically nanopatterned (red), randomly textured (black) or flat (gray).

#240779 Received 12 May 2015; revised 19 Sep 2015; accepted 12 Oct 2015; published 23 Oct 2015

contact texture. Analyzing the optical response for wavelengths longer than 550 nm, the flat solar cell shows the lowest absorptance and *EQE*, since it only shows a negligible light trapping effect. In contrast to the results of the flat solar cell, the *EQE* and *A* of the randomly textured back contact is strongly increased over the entire spectral range. Towards longer wavelengths, a smooth and steady decreasing *EQE* can be observed. Significantly different measurement results are found for the thin-film solar cell with *PRGBC*. In evidence, the results support the claim that solar cells with adjusted periodic nanopatterns can trap light superior to randomly textured devices. Most obvious in the wavelengths range between 500 nm and 600 nm, the *EQE* is increased compared to the randomly textured device. For longer wavelengths, multiple spectrally fairly sharp resonances are resolved in the *EQE*. In particular in the wavelength range between 650 nm and 780 nm seven maxima are resolved. These maxima raise due to coupling incident light to leaky waveguide modes, as explained before [20,21].

Surprisingly, comparing *A* and *EQE*, a significant shift of around 10 nm between the spectral positions of some resonances can be found. This is an important observation as far as the only varied parameter between both setups is the angle of incidence, which differs less than ten degrees. For the following investigation this observation already demonstrates the strength of the angular dependence of the periodically nanopatterned solar cells. For this reason, our detailed analysis is necessary.

Since we found variations in the optical response of the devices with different light trapping concepts, shown in Fig. 1, also the short-circuit current densities (J_{SC}) eventually differ. A detailed summary of the properties of our devices can be found in Table 1. It can be seen that for a flat solar cell, the resulting J_{SC}, determined from *EQE* measurements, is 12.5 mA/cm^2. The J_{SC} increases up to 14.7 mA/cm^2 and 14.9 mA/cm^2 for the randomly textured solar cell and the periodically nanopatterned solar cell, respectively. The fill factor (*FF*) and open-circuit voltage (V_{OC}) are measured by a sun simulator system. As the solar cell area is not defined by laser texturing, the measurements are typically done with shadow masks, covering the surrounding area, to prevent current collection. For technical reasons the periodically textured device was measured without mask and therefore the V_{OC} is increased but the *FF* is reduced.

In case, the focus of this study is on the light-trapping effect of the thin-film solar cells, concentrating on coupling incident light to leaky waveguide modes. Therefore, the J_{SC} is the significant measure to us and is always calculated from *EQE* measurements. Using the presented results we calculate the initial power conversion efficiency η. It can be seen, that the highest η is given by the randomly textured thin-film solar cell, followed by the periodically textured one and the flat one. It should be mentioned that during this study, also periodically textured thin-film solar cells showing enhanced η compared to a randomly textured thin-film solar cell were found. These results have been reported elsewhere [21].

Table 1. Fill factor, open-circuit voltage, short-circuit current density and power conversion efficiency of hydrogenated amorphous silicon thin-film solar cells with an i-layer thickness of 280 nm deposited on various substrates

Back contact	*Fill factor (FF)*	*Open-circuit voltage* (V_{OC}) [mV]	*Short-circuit current density* (J_{SC})[mA/cm²]	*Power conversion efficiency* (η)
Periodic	0.65	912	14.9	8.8
Random	0.72	870	14.7	9.1
Flat	0.70	890	12.5	7.8

#240779 Received 12 May 2015; revised 19 Sep 2015; accepted 12 Oct 2015; published 23 Oct 2015

3.2. Angle dependent coupling of light to leaky waveguide modes in periodically nanopatterned solar cells

As the next step in our study, we reproducibly observe a shift of the resonances' wavelengths with increasing angle of incidence of the illumination. This effect is such strong that the spectral shifts of the resonances can already be observed in tilting steps of 4°.

Figure 2(a) shows a sketch of the applied experimental setup. A thin-film solar cell illuminated with light polarized linearly in x-direction (p-polarized) is shown. The polarization direction is along the grating vector of the nanopattern. For the analyzed sample, the period of the nanopattern is 500 nm in x-direction and y-direction.

For this nanophotonic sample the *EQE* is determined with a spectral resolution around 3 nm for tilting angles in steps of 4°. This rather high spectral resolution is required for the analysis of the spectral position of the resonances. The results are shown in Fig. 2(b).

The observed spectral shift is related to the variation of the diffraction angles at the *PRGBC*, which in turns influences the wavelength of light coupling to individual leaky waveguide modes [18,22]. The explanation can be given by the conditions for a standing wave inside a planar waveguide described by:

$$\frac{2\pi}{\lambda}\cdot n\cdot 2d\cdot\cos(\alpha)+\phi+\pi=2\pi\cdot m \qquad (1)$$

where n is the refractive index of the wave guiding layer, λ is the resonance wavelength, d is the waveguide thickness, α is the angle of incidence, ϕ is the phase shift of the electromagnetic wave at the dielectric-air-interface and *m* is an integer related to the waveguide modes. It can be seen that the right hand side of the Eq. (2)π m) is independent for variations of the angle of incidence. On the left hand side, the cos(α) decreases for such variations. In order to keep the right hand side constant increasing angles of incidence will mainly have to be compensated by shorter λ. This explains the spectral shift of the wavelengths where light couples to leaky waveguide modes for various angles of incidence. In order to underline the impact of the angle of incidence on the spectral positions of coupling light to leaky waveguide modes, we next characterize the *EQE* of the solar cells polarization dependent. The two limiting cases are light polarized parallel to the x-direction (p-polarized) and y-direction (s-polarized) at normal incidence. The sample is measured after a rotation of 8° around the y-axis (see Figs. 3(a) and 3(b)). We investigate the behavior of a solar cell in steps of 10° in polarization. In this contribution, we define the p-polarized and s-polarized light as 0° and 90°, respectively. Superposition allows distinguishing between light coupling to leaky waveguide modes in x-direction and in y-direction. Figure 3(c) shows the experimental data, i.e. the *EQE* and *A*. The maximum polarization directions applied during the EQE measurements are marked in black and red, here 0° and 90° polarization, respectively. Spectrally sharp maxima are resolved and the *EQE* and *A* are in a very good agreement. The continuous transfer from 0° polarization in black to 90° in polarization in red can be observed. These measurements support the extremely sensitive optical response of the coupling of light to leaky waveguide modes between 650 nm and 750 nm. In particular, we show that the polarization of the incident light influences the spectral position of leaky waveguide modes for tilted samples.

#240779 Received 12 May 2015; revised 19 Sep 2015; accepted 12 Oct 2015; published 23 Oct 2015

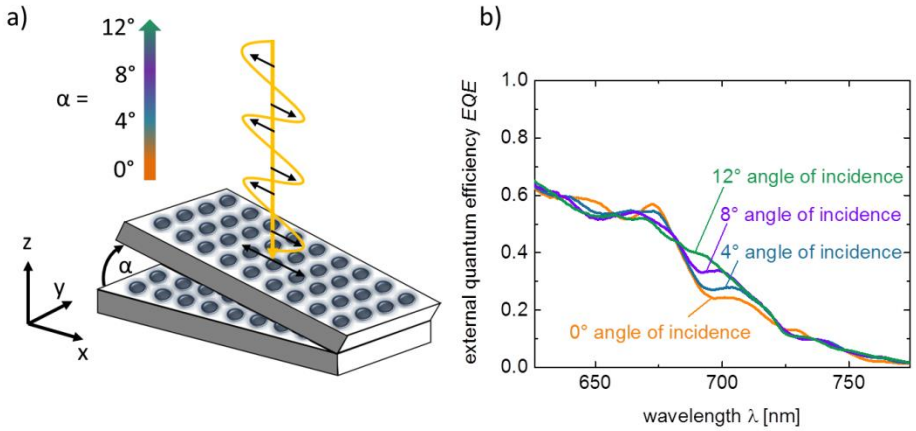

Fig. 2. a) Scheme of a thin-film solar cell illuminated with light polarized in x-direction. The sample is tilted between zero and twelve degrees using the y-axis as rotation axis. b) *EQE* of a thin-film solar cell processed on a *PRGBC* with a period of 500 nm measured under different angles of incidence.

3.3. Disorder in periodically nanopatterned back contacts

From literature, it is known that introducing disorder to initially periodically nanopatterned p I n solar cells can improve the overall light trapping for normal angle of incidence [20]. Similar trends like in this study were also found for our solar cells in n-i-p configuration. Having demonstrated a strong angular dependence of coupling light to leaky waveguide modes of periodically nanopatterned thin-film solar cells, we study the impact of disorder on this angular dependency. In order to realize an accurate analysis, we focus on the angular dependent optical response of light trapping of the prototype solar cells with only three kinds of back contacts: (i) Commercially available disordered, (ii) perfectly periodically arranged and (iii) one specific amount of introduced disorder.

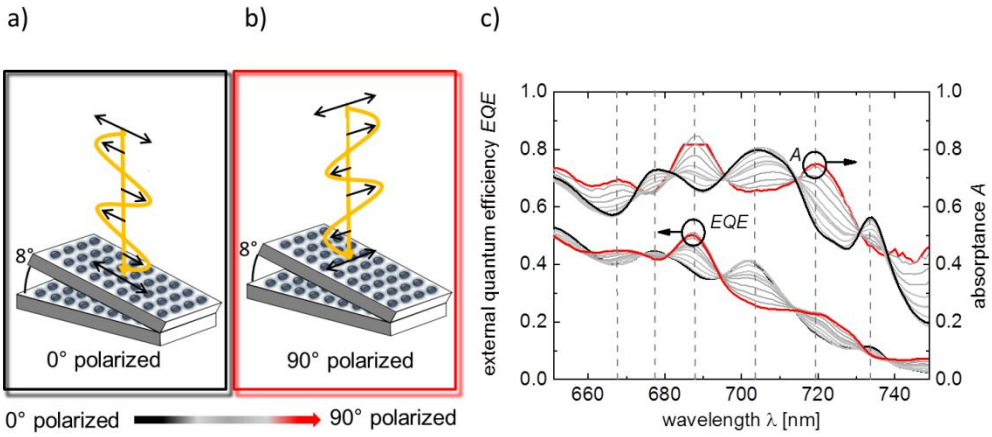

Fig. 3. a) Scheme of a thin-film solar cell illuminated with light polarized in x-direction (0° polarization). b) Scheme of a solar cell with light polarized parallel to the y-direction (90° polarized). c) External quantum efficiency (*EQE*) and absorptance (*A*) of a hydrogenated amorphous silicon thin film solar cell processed on a *PRGBC* with a period of 500 nm. The polarization is varied in steps of 10° between 0° (black line) and 90° (red line). The sample is rotated around the y-axis by 8°.

#240779 Received 12 May 2015; revised 19 Sep 2015; accepted 12 Oct 2015; published 23 Oct 2015

Introducing disorder induces a stochastic variation of the position of nanostructures according to a Gaussian distribution. In Fig. 4(a), the Gaussian distribution function is shown as a function of the displacement of nanostructures from the perfect position of a periodically nanopatterned *PRGBC*. The corresponding curves are labeled by a *SEM* image of a corresponding surface morphology of the back contact. For a periodically nanopatterned back contact, the relative standard deviation (σ_{rel}) of the period is 0% and therefore 0 nm, whereas the position of the disordered nanostructures can vary. It can vary around 100 nm in all surface directions applying σ_{rel} = 12%, if we assume the full-width-half-maximum position of the corresponding Gaussian distribution. In the following, we compare solar cells with these kinds of nanophotonic back contacts. We will see that the *EQE* of the disordered back contact is improved over a significant wavelength-range compared to the periodically nanopatterned back contact, especially for large angles. Representative *EQEs* of such devices are shown in Fig. 4(b) as a function of the wavelength. For wavelengths shorter than 550 nm, the *EQEs* are almost identical.

Due to coupling light to leaky waveguide modes in the periodically nanopatterned thin-film solar cell, we observe sharp resonances around 660 nm, 700 nm and 735 nm when investigating longer wavelengths. For devices with disordered *PRGBC,* these resonances broaden and their intensity reduces because of the weakened resonance conditions and the broadened wave vector transfer. Overall, the *EQE* is slightly enhanced compared to the thin-film solar cell with periodically textured back contact for wavelengths longer than 550 nm. Solely at the resonance positions exceptions appear. This fact results in an enhancement of the J_{SC} of around 0.3 mA/cm^2 for the disordered back contact. Such an effect was shown by Paetzold et al. for a-Si:H thin-film solar cells in superstrate configuration with dielectric, TCO coated, gratings acting as front contact, before [20]. As a first step, we investigate the angular dependence of the absorptance of such a device with disordered *PRGBC.* We use the same measurement setup as applied before. Figures 5(a) and 5(b) show the applied setup to recap. In Fig. 5(c), we, again, see the absorptance during the continuous transfer from 0° polarization (black line) to 90° polarization (red line). Interestingly, the variations in between these two measurement curves are heavily reduced, as compared to the perfect periodic structure in Fig. 3(c). This means disordered nanostructures reduce the polarization dependence of the absorptance, compared to a periodically nanopatterned back contact. This raises the question if also the spectral response of solar cells is increasingly angle insensitive when applying disordered nanostructures.

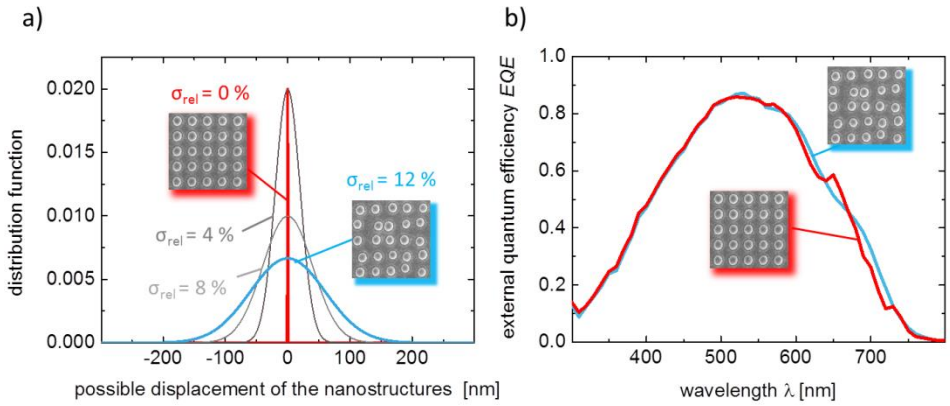

Fig. 4. a) Gaussian distribution function of the possible displacement of nanostructures from the positions for a perfectly periodic arrangement. b) External quantum efficiency (*EQE*) of thin-film solar cells processed on plasmonic reflection grating back contacts (*PRGBC*) with a period of 500 nm and a relative standard deviation (σ_{rel}) of zero percent and twelve percent under normal incidence in all direction.

#240779 Received 12 May 2015; revised 19 Sep 2015; accepted 12 Oct 2015; published 23 Oct 2015

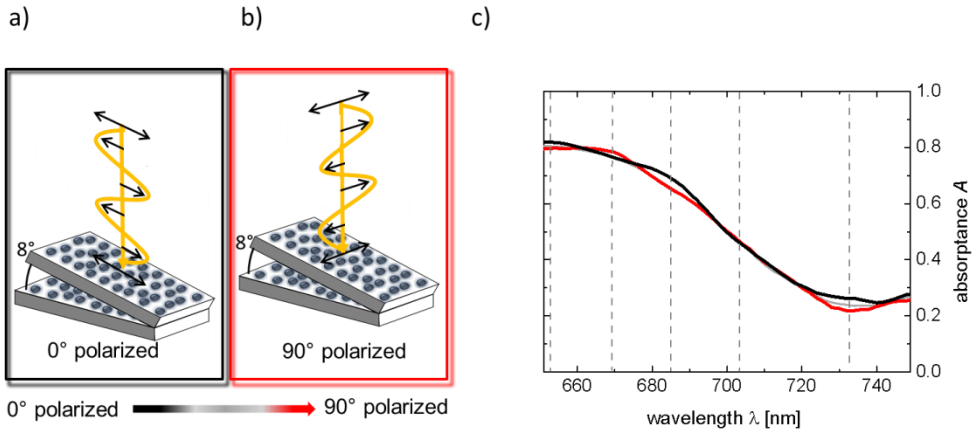

Fig. 5. a) Scheme of a thin-film solar cell illuminated with light polarized in x direction (0° polarized) at an angle of incidence of eight degrees. b) Scheme of a solar cell with light polarized in y direction (90° polarized). c) Absorptance (*A*) of a hydrogenated amorphous silicon thin film solar cell processed on disordered plasmonic reflection grating back contacts (*PRGBC*) with a period of 500 nm under different polarizations.

3.4. Characteristics of the angular dependence of nanophotonic light trapping

We showed the strong angular dependence of coupling incident light to leaky waveguide modes in a-Si:H thin-film solar cells. This raises the important question of whether this angular dependence causes problems for the implementation in a solar cell module, if the device is not tracking the position of the sun, which would guarantee normal incidence. For this reason, the following part is concerned with a detailed comparison of the impact of the angular dependence of our devices on *EQE* and the corresponding J_{SC}. The compared solar cells are deposited on: (i) randomly textured substrates, (ii) periodically nanopatterned substrates and (iii) nanopatterned substrates with disorder.

In this contribution, the *EQE* of the solar cells is determined for light polarized in x direction and y direction of the device along the grating vectors. The angle of incidence is varied between 0° and 75° around the y-axis of the device. To be sure that measurement conditions kept constant and Staebler-Wronski degradation did not take place the 0° measurement was performed twice. One measurement took place at the beginning and one at the end of every experiment. No changes were observed.

From these measurements, we calculate the Δ *EQE*, defined as:

$$\Delta EQE(\alpha,\lambda) = EQE(\alpha,\lambda)/EQE(0°,\lambda) - 1 \qquad (2)$$

where α is the angle of incidence and λ is the wavelength of the incident light. We calculate Δ *EQE* to amplify the signatures of leaky waveguide modes in the *EQE* measurements. In Fig. 6, the Δ *EQE* of thin-film solar cells with the three different back contacts is plotted in a color code as a function of the wavelength and the angle of incidence. The angular resolution is 5°, values in between the measurement points are interpolated.

#240779 Received 12 May 2015; revised 19 Sep 2015; accepted 12 Oct 2015; published 23 Oct 2015

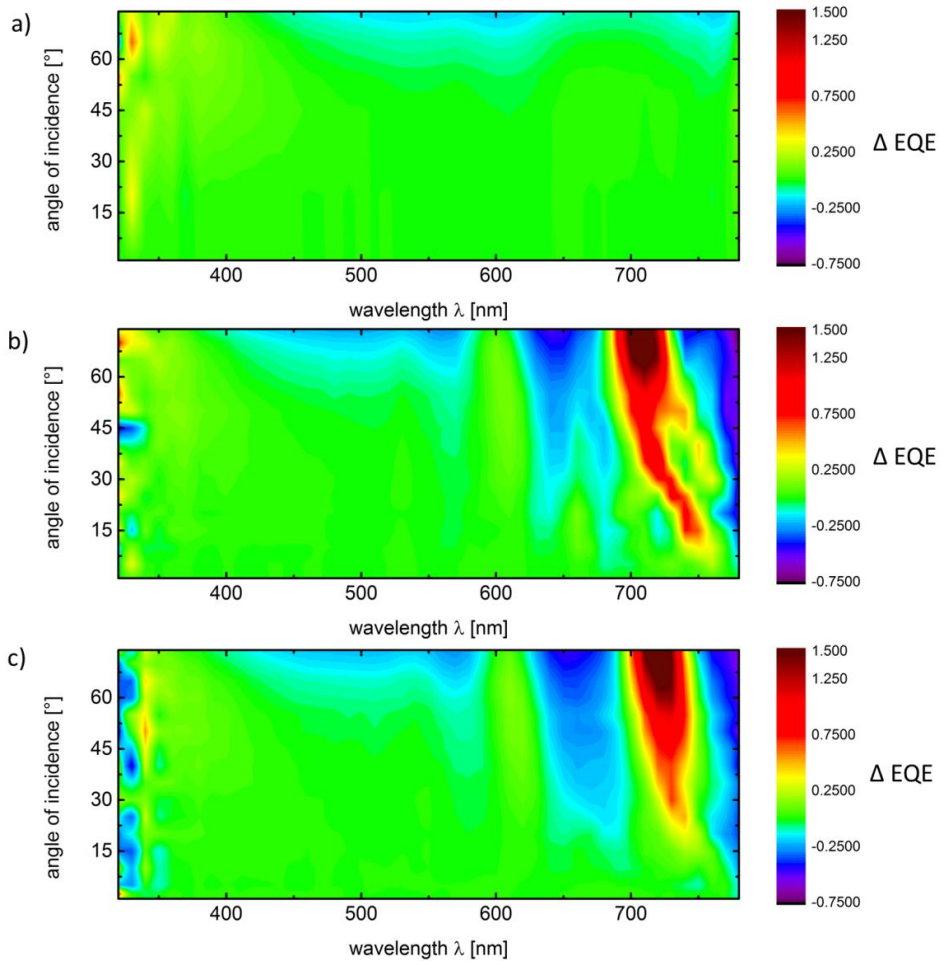

Fig. 6. a) Δ External quantum efficiency (*EQE*) as a function of the wavelength and the angle of incidence in the wavelength-range between 360 nm and 790 nm of hydrogenated amorphous thin-film solar cells. The solar cells are deposited on (a) a randomly textured substrate, (b) a periodically structured and (c) a structured substrate with a σ_{rel} of 12%. The incident light is polarized in x-direction.

Figure 6(a) shows the Δ *EQE* of a thin-film solar cell with randomly textured back contact in the wavelength-range between 360 nm and 790 nm. The light-trapping concept is based on random scattering, which is not directed and results only in small changes in Δ *EQE* [28,29]. Contrary, the Δ *EQE* of a thin-film solar cell with periodically nanopatterned back contact is shown in Fig. 6(b). Comparing Figs. 6(b) and 6(a) between 300 nm and 600 nm shows that the Δ *EQE* differs just little for both thin-film solar cell concepts.

For wavelengths longer than 600 nm, remarkable features in the Δ *E*QE of the nanopatterned solar cells occur. Obviously, the features occur due to the variation of the spectral position of leaky waveguide modes. Features are formed for angles between 5° and 75°, due to the sharp effective wave vector transfer of the periodic grating. Most notably is the dominant waveguide mode (red area) shifting from around 750 nm to around 720 nm. Such shifts of waveguide modes could end up in reduction or enhancement of the J_{SC}. Consequently, we are aiming at a reduction of this angular dependence by introducing disorder to the initially periodically nanopatterned back contacts. By introducing disorder we broaden the wave vector transfer due to reduced periodicity of the grating. This allows for light coupling to leaky waveguide modes for a broader spectral range.

#240779 Received 12 May 2015; revised 19 Sep 2015; accepted 12 Oct 2015; published 23 Oct 2015

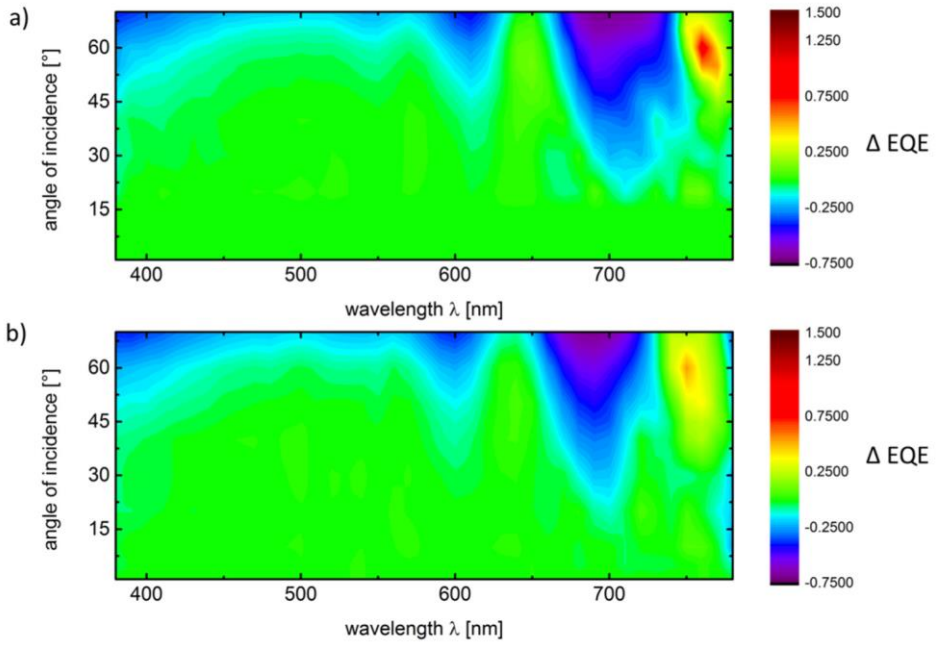

Fig. 7. Δ External quantum efficiency (*EQE*) as a function of the wavelength and the angle of incidence in the wavelength-range between 360 nm and 790 nm of hydrogenated amorphous thin-film solar cells. a) for a periodically structured thin-film solar cell and b) a thin-film solar cell with disordered structures with a σ_{rel} of twelve percent; Incident light is polarized in y direction

Taking Fig. 6(c) in consideration, the same parameters are plotted for a thin-film solar cell with disordered back contact. We directly focus on the wavelengths longer than 600 nm, which are interesting for light trapping. As expected, the angular dependence of coupling light to leaky waveguide modes is reduced by increasing disorder. In contrast to the randomly textured solar cells, features like for periodically nanopatterned solar cells occur in the Δ *EQE*. But, compared with the periodically nanopatterned solar cells, these features of leaky waveguide modes broaden. As one example for the reduced angular dependence of waveguide coupling, the waveguide mode shifting from around 750 nm to 720 nm should be mentioned. It can be seen that this resonance is formed, for the periodically textured back contact and also for the disordered back contact. The difference between the light-trapping effects can be found in the angles of incidence, where this mode starts shifting significantly. For the periodically nanopatterned back contact, shifting starts at 5°, while for the disordered back contact, it only takes place for angles larger than 20°. In conclusion, we find a decreased dependence of the disordered back contact on the angle of incidence.

In the next section, we turn the polarization to 90°. It is now parallel to the grating vector in y-direction. Still, the sample is tilted 8 degrees in x direction. Corresponding measurements of the Δ *EQE* are shown in Fig. 7. Compared to Fig. 6 we dispense with the randomly textured back contact, as no significant variations can be observed comparing normal incidence and 60° angle of incidence over the complete wavelength range for this system.

The plots in Figs. 6 and 7 differ significantly for both polarization directions. Figure 7 shows, that there are no significant variations of the Δ *EQE* for angles smaller than 20° between 360 nm and 790 nm. This result is independent of the type of nanophotonic back contact. For wavelength shorter than 600 nm the Δ *EQE* lowers with increasing angle of incidence. This effect is known to occur for thin-film solar cells. One of the reasons is the enhanced light path inside the TCO, causing enhanced parasitic absorptance. Another reason

#240779 Received 12 May 2015; revised 19 Sep 2015; accepted 12 Oct 2015; published 23 Oct 2015

is increasing reflectance of light at the front contact. This means incoupling into the solar cell at different angles is independent of the type of analyzed nanophotonic back contact.

For longer wavelengths, two dominant resonances form in this spectral range. Interestingly, this behavior was also observed for flat thin-film solar cells deposited similarly to the nanophotonic thin-film solar cells. The only resonances in flat solar cells can be Fabry-Pérot resonances. Therefore, our interpretation is that also for the periodically nanopatterned solar cells Fabry-Pérot resonances become dominant when illuminated under large angles of incidence.

3.5. The angular dependence of the short-circuit current density applying nanophotonic light trapping structures

Having experimentally shown the angular dependence of the spectral shift of coupling light to leaky waveguide modes applying nanophotonic back contacts, we investigate variations in the generated J_{SC} of the thin-film solar cells. The J_{SC} of the solar cells is determined under various angles of incidence. Different to the recent results, we are comparing results for unpolarized light here.

We calculate the ratio $\Delta J_{SC} = J_{SC}(\alpha) / J_{SC}(0)$ from *EQE* in the wavelength range between 360 nm and 800 nm. ΔJ_{SC} is plotted as a function of the angle of incidence up to 75° for the three different types of back contacts in Fig. 8. Again, thin-film solar cells applying randomly textured back contacts are used as reference. A possible reduction of the angular dependent variations of the J_{SC} compared to randomly textured solar cells could enhance the relevance of nanophotonic light-trapping concepts.

For the randomly textured solar cell (red circles), the J_{SC} is weakly enhanced up to an angle of incidence of 40°. Taking measurement errors in consideration, we should not go beyond taking this J_{SC} as constant. Nonetheless, the raw data support the fact that this enhancement is caused by a little improvement of incoupling the light into the solar cell at short wavelengths. For larger angles of incidence, the J_{SC} lowers continuously. In detail, the J_{SC} at 75° is reduced around 15% of the J_{SC} at 0°. One of the reasons is the enhanced reflection at the air-glass interface.

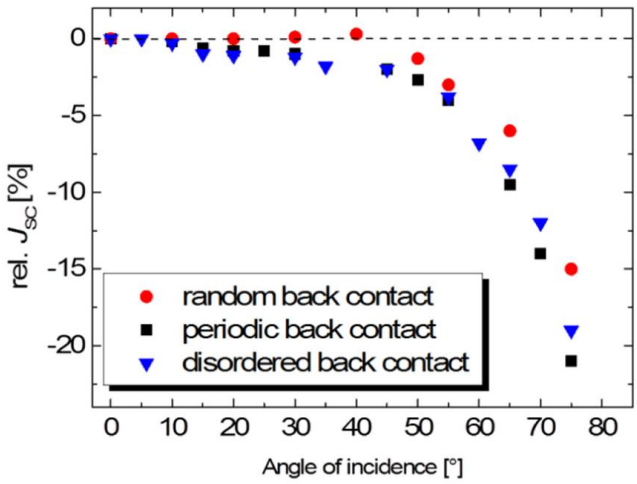

Fig. 8. Short-circuit current density (rel. J_{SC}) of hydrogenated amorphous thin-film solar cells with a thickness of the i-layer of 280 nm as a function of the angle of incidence normalized to the short-circuit current density for an angle of incidence of 0°. The solar cells are deposited on a periodically textured substrate, a textured substrate with a σ_{rel} of twelve percent and a randomly textured substrate.

#240779 Received 12 May 2015; revised 19 Sep 2015; accepted 12 Oct 2015; published 23 Oct 2015

The behavior slightly differs for thin-film solar cells with nanophotonic back contact. For both, periodically nanopatterned and disordered back contacts, the J_{SC} continously decreases towards increasing angles of incidence. For the nanophotonic prototype solar cells, the rel. J_{SC} is not enhanced under any angle of incidence compared to the randomly textured solar cell. In detail, the J_{SC} of the nanophotonic solar cells decrease similarly between 0° and 55°. Towards larger angles of incidence, the periodically nanopatterned solar cells show weaker $\Delta J_{SC.}$ As a result, the periodically nanopatterned solar cells show the strongest reduction of the short-circuit current density, followed by disordered solar cells and randomly textured solar cells.

One of the reasons is the increasingly insensitive wave vector transfer, caused by the disorder and random textures. As explained introducing disorder results in broadening of the waveguide resonances and a reduction of the angular sensitivity of light trapping. Still the rel. J_{SC} of the devices with disordered back contact is stronger reduced than for randomly textured devices. Future studies will have to show if a reduction of the angular dependence in initially periodically nanopatterned back contacts by disorder can be improved even more. One route to improve the angular insensitivity of light trapping we found here, is introducing a defined amount of disorder.

Conclusions

In conclusion, we investigated the angular sensitivity of light trapping in amorphous thin-film silicon solar cells in substrate configuration processed on different types of back contacts. These back contacts are either (i) periodically nanopatterned, (ii) intentionally disordered patterned or randomly textured. In detail, we varied the angle of incidence and polarization direction of the illumination and determine the corresponding *EQEs* and short-circuit current densities of the solar cells. We find that light trapping in solar cells made of hydrogenated amorphous silicon applying periodically nanopatterned back contacts depends strongly on the angle of incidence. With changing angle of incidence, the spectral positions of resonances, which are the result of coupling light to leaky waveguide modes, vary. We determine the spectral shift in *EQE* as well as absorptance. Overall, the shift of the spectral position results in variations of the short-circuit current density. To improve light trapping and the angular sensitivity of coupling light to leaky waveguide modes, we intentionally introduce disorder to the nanopatterned back contacts. Other studies have shown the potential to improve light trapping by introducing disorder. Also our solar cells with disorder show an improved light-trapping effect and we investigated the behavior for angles up to 75°. As a result, we found that introducing disorder is not only a promising method for enhancing the short-circuit current density of such solar cells, but also a method to reduce the angular sensitivity of the J_{SC} at large angles. This sensitivity is known for thin-film solar cells with periodically nanopatterned back contacts. The results suggest that disorder is one route to follow in order to process nanophotonic solar cells with low angular sensitivity of the short-circuit current densities aiming at high power conversion efficiencies. As we used amorphous silicon with growth conditions close to other thin-film absorber materials we assume the results to be tuneable due to optimizations of the absorber thickness. In addition, we expect the possibility of a transfer to other thin-film materials like CIGS or organic absorbers.

Acknowledgment

The authors acknowledge the project Infravolt for financial support. Special thanks go to Wilfried Reetz and Thomas Birrenbach for excellent support during the DSR setup modifications. We also thank Alain Doumit, Oleg Tremmel, Hilde Siekmann and Ulrike Gerhards.

#240779 Received 12 May 2015; revised 19 Sep 2015; accepted 12 Oct 2015; published 23 Oct 2015